Green Synthesis and Comprehensive Characterization of Zinc Oxide Nanoparticles Using *Alternanthera sessilis* Leaf Extract

Chakravarthi Booravilli[1,2], Padmavathi Pamulapati[2], Vasantha Lakshmi Mamillapalli[2],[3]

[1]Department of Zoology, Pithapur Rajah's Government College (A), Kakinada, Andhra Pradesh, India.
E-Mail: chakrizoologist@gmail.com
[2]Department of Zoology & Aquaculture, Acharya Nagarjuna University, Guntur, Andhra Pradesh, India
[3]Department of Zoology, A.S.D. Government Degree College for Women(A), Kakinada, India

Abstract
Green synthesis of metal oxide nanoparticles using plant extracts has emerged as an environmentally friendly alternative to conventional chemical methods. In the present study, zinc oxide (ZnO) nanoparticles were synthesized using the aqueous leaf extract of Alternanthera sessilis. Preliminary phytochemical screening confirmed the presence of flavonoids, terpenoids, anthraquinones, and glycosides, which acted as reducing and stabilizing agents during nanoparticle synthesis. The synthesized ZnO nanoparticles were characterized using UV–Visible spectroscopy, FTIR, XRD, FESEM-EDAX, HRTEM, dynamic light scattering (DLS), and zeta potential analyses. The UV–Visible spectrum exhibited strong absorption in the ultraviolet region, confirming the semiconducting nature of ZnO nanoparticles. FTIR analysis revealed hydroxyl, carbonyl, and other oxygen-containing functional groups involved in nanoparticle formation and stabilization. XRD analysis confirmed the formation of highly crystalline hexagonal wurtzite ZnO with an average crystallite size of 22.8 nm. FESEM and HRTEM analyses showed predominantly spherical to quasi-spherical nanoparticles with particle sizes ranging from 3–35 nm. EDAX confirmed zinc and oxygen as the major constituent elements, indicating high purity of the synthesized nanoparticles. DLS and zeta potential analyses demonstrated moderate colloidal stability with particle aggregation in aqueous suspension. The results demonstrate that A. sessilis leaf extract is an effective natural reducing and capping agent for the eco-friendly synthesis of crystalline ZnO nanoparticles with promising potential for photocatalytic and biomedical applications.

Keywords: Alternanthera sessilis; Green synthesis; Zinc oxide nanoparticles; Phytochemical screening

1. Introduction

Nanotechnology studies and engineers materials at roughly 1–100 nm, where size-dependent optical, mechanical, electrical, and chemical properties enable applications across medicine, energy, electronics, environmental science, and engineering [1–3]. Green nanomaterials extend this field by applying green chemistry to nanoparticle synthesis, replacing hazardous, energy-intensive physical and chemical routes with plant, microbial, or other biological systems that act as reducing, capping, and stabilizing agents [4,5]. Compared with conventional methods, green synthesis is described as more eco-friendly, lower-toxicity, and often lower-cost, with reduced energy demand and stronger alignment with sustainable manufacturing and circular-economy goals [4,6]. Plant extracts are especially prominent because phytochemicals such as flavonoids, phenols, terpenoids, proteins, and alkaloids can drive metal-ion reduction while also stabilizing nanoparticle growth and morphology [5,7,8]. These green nanomaterials already show broad potential in drug delivery, biosensing, cosmetics, water treatment, pollutant remediation, antimicrobial technologies, agriculture, and energy storage, although the literature still identifies major challenges in scale-up, reproducibility, mechanism, and toxicity standardization before routine large-scale adoption [2].

Zinc oxide nanoparticles (ZnO NPs) synthesized through green methods have attracted strong research interest because conventional physical and chemical routes often require hazardous reagents, higher energy input, or costly processing, whereas plant-mediated synthesis is simpler, safer, and more environmentally compatible [9–11]. In green synthesis, plant extracts from leaves, fruits, seeds, roots, or whole plants provide phytochemicals such as phenolics, flavonoids, alkaloids, and terpenoids that act as reducing, capping, and stabilizing agents during nanoparticle formation [12]. This biofabrication route is valued for its cost-effectiveness, reduced toxicity, biocompatibility, and lower waste generation, although true green synthesis should avoid auxiliary toxic solvents or chemicals that undermine green-chemistry principles [13].

For *Alternanthera sessilis* leaf-mediated synthesis, the rationale is that leaf phytochemicals can direct ZnO NP formation while influencing crystallinity, morphology, particle size, and surface properties, which in turn shape biological and catalytic performance [12,14]. ZnO NPs are especially attractive because they combine low toxicity and biodegradability with broad functionality in antimicrobial, antioxidant, anti-inflammatory, anticancer, sensing, and photocatalytic applications [9,14,15]. Characterization therefore becomes essential, and green-synthesized ZnO NPs are commonly verified by UV-Vis spectroscopy, Fourier transform infrared (FTIR) spectroscopy, X-ray diffractometer (XRD), electron microscopy, Zeta size, and elemental analysis to confirm ZnO formation, wurtzite crystallinity, nanoscale size, morphology, and phytochemical surface capping. Across plant-based studies, the resulting ZnO NPs have shown promising applications in antibacterial control, enzyme-related biomedical uses, dye degradation, wastewater remediation, and environmental catalysis, which supports investigating *A. sessilis* leaves as a sustainable precursor for producing functional ZnO nanomaterials [16,17].

Till date the ZnO NPs synthesized using *A. sessilis* showed effective *in vitro* biological activities. Therefore, further *in vivo* assays required to determine the efficacy of ZnO NPs synthesized using *A. sessilis*.

Thus the objectives of the present study are:
1. To collect the *A. sessilis* leaves from Kakinada, Andhra Pradesh India.
2. To synthesize the ZnO NPs using *A. sessilis* leaf aqueous extract
3. To evaluate the optical properties of synthesized ZnO NPs using UV-Vis spectroscopy and FTIR
4. To evaluate the phase analysis, morphology, size distribution of synthesized ZnO NPs using XRD, FESEM-EDAX, HRTEM and Zeta Size.

2. Material and Methods

2.1 Collection and Processing of *Alternanthera sessilis* Leaves

Fresh leaves of *Alternanthera sessilis* were collected from in and around Kakinada, Andhra Pradesh, India. The collected leaves were washed thoroughly with tap water followed by distilled water to remove dust and other impurities. The leaves were shade-dried at room temperature until completely dry. The dried leaves were then ground into a fine powder using an electric grinder and stored in an airtight container until further use.

2.2 Preparation of *Alternanthera sessilis* Aqueous Extract

The aqueous extract of *Alternanthera sessilis* leaves was prepared using a simple decoction method. Briefly, 5 g of the dried leaf powder was mixed with distilled water and heated at 60°C for 1 h. After cooling to room temperature, the extract was filtered through Whatman No. 1 filter paper to remove plant debris. The filtrate was collected and stored at 4°C until further use in the experimental studies.

2.3. Preliminary qualitative phytochemical screening

Preliminary qualitative phytochemical screening of the *Alternanthera sessilis* aqueous leaf extract was carried out using standard phytochemical procedures to determine the presence or absence of major secondary metabolites. Flavonoids were detected using the alkaline reagent test, phenols by the ferric chloride test, tannins by the ferric chloride test, alkaloids by Mayer's test and Wagner's test, terpenoids by the Salkowski test, anthraquinones by the Bornträger's test, saponins by the foam test, quinones by the concentrated sulfuric acid test, coumarins by the sodium hydroxide test, glycosides by the Keller–Killiani test, and steroids by the Liebermann–Burchard test. The development of characteristic colour changes or precipitates was recorded as an indication of the presence of the respective phytochemical constituents.

2.4 Green Synthesis of Zinc Oxide (ZnO) Nanoparticles

Zinc oxide (ZnO) nanoparticles were synthesized using the aqueous leaf extract of *Alternanthera sessilis* through a green synthesis approach. Briefly, 10 mM zinc chloride ($ZnCl_2$) solution was prepared in distilled water, and 90 mL of the precursor solution was transferred to a 250 mL beaker. The solution was heated at 70°C under continuous magnetic stirring for 20 min to ensure complete dissolution of the precursor. After the initial heating period, 10 mL of the freshly prepared aqueous leaf extract was added dropwise to the zinc chloride solution while maintaining the temperature at 70°C. The reaction mixture was continuously stirred for an additional 20 min to facilitate the interaction between the zinc ions and the phytochemicals present in the plant extract. The reaction was then allowed to continue at 70°C for 2 h under constant stirring to promote the formation of zinc oxide nanoparticles. Following the reaction, 10 mL of 10% (w/v) sodium hydroxide (NaOH) solution was added slowly to the reaction mixture under continuous stirring until a white precipitate was formed. The resulting suspension was centrifuged at 5000 rpm for 5 min, and the supernatant was discarded. The collected precipitate was washed three times with distilled water followed by three washes with 70% ethanol to remove unreacted precursors and residual phytochemicals. Finally, the purified ZnO nanoparticles were dried in a hot-air oven at 60°C overnight. The dried powder was gently ground using a mortar and pestle and stored in airtight containers for further characterization

2.5 Characterization of Optical Properties

The optical properties of the synthesized samples were characterized using ultraviolet-visible (UV-Vis) spectroscopy and Fourier transform infrared (FTIR) spectroscopy.

2.5.1 UV-Visible Spectroscopy

The optical absorption spectrum of the synthesized sample was recorded using a Shimadzu UV-2600 UV-Visible spectrophotometer**.** Before analysis, the sample was dispersed in distilled water by sonication for 10 min to obtain a uniform suspension. The spectrum was recorded in the wavelength range of 200–800 nm using distilled water as the reference blank. The absorption peaks obtained from the spectrum were used to identify the characteristic electronic transitions and to evaluate the optical behavior of the synthesized material.

2.5.2 Fourier Transform Infrared (FTIR) Spectroscopy

The surface functional groups present in the synthesized sample were identified using a Bruker Alpha II Fourier Transform Infrared (FTIR) spectrometer**.** The dried sample was analyzed directly using the ATR (Attenuated Total Reflectance) mode. The FTIR spectrum was recorded in the range of 4000–400 cm^{-1} with a spectral resolution of 4 cm^{-1} by averaging 32 scans. The absorption bands were used to identify the major functional groups responsible for the reduction, stabilization and surface capping of the synthesized material.

2.6 Phase Analysis, Morphology and Size Distribution

2.6.1 X-ray Diffraction (XRD)

The crystalline nature and phase composition of the synthesized sample were analyzed using a Bruker D8 Advance X-ray diffractometer equipped with Cu-Kα radiation (λ = 1.5406 Å)**.** The diffraction pattern was recorded over a 2θ range of 10°–80° with a scanning rate of approximately 2° min^{-1}**.** The diffraction peaks obtained were compared with standard JCPDS database files to identify the crystalline phase. The average crystallite size was estimated using the Debye–Scherrer equation:

$$D = K\lambda / \beta \cos \theta$$

where D is the crystallite size, K is the shape factor (0.9), λ is the X-ray wavelength (1.5406 Å), β is the full width at half maximum (FWHM) of the diffraction peak, and θ is the Bragg diffraction angle.

2.6.2 Field Emission Scanning Electron Microscopy and Energy Dispersive X-ray Analysis (FESEM-EDAX)

The surface morphology and elemental composition of the synthesized sample were examined using a JEOL Field Emission Scanning Electron Microscope (FESEM) equipped with an Energy Dispersive X-ray Analysis (EDAX) detector. A small quantity of the dried sample was mounted on carbon tape fixed to an aluminium specimen stub and coated with a thin layer of gold to improve electrical conductivity. The FESEM images were recorded at different magnifications to observe the particle morphology, while EDAX analysis was performed to determine the elemental composition and confirm the presence of the constituent elements in the synthesized material.

2.6.3 High-Resolution Transmission Electron Microscopy (HRTEM)

The particle size, morphology and internal crystal structure of the synthesized sample were investigated using a Thermo Scientific High-Resolution Transmission Electron Microscope (HRTEM)**.** A dilute suspension of the sample was prepared in distilled water and sonicated for 10 min. A few microlitres of the suspension were placed on a carbon-coated copper grid and allowed to dry at room temperature before analysis. The HRTEM images were recorded to determine particle size, particle shape and lattice fringes. Selected Area Electron Diffraction (SAED), when available, was used to confirm the crystalline nature of the synthesized material.

2.6.4 Dynamic Light Scattering (DLS) and Zeta Potential Analysis

The hydrodynamic particle size distribution and surface charge of the synthesized sample were determined using a Malvern Zetasizer Nano ZS90. The sample was dispersed in distilled water and sonicated for 10 min to obtain a homogeneous suspension. The measurements were carried out at 25°C using disposable cuvettes for particle size analysis and folded capillary cells for zeta potential measurements. The average hydrodynamic diameter, polydispersity index (PDI) and zeta potential values were recorded to evaluate the particle size distribution, dispersion uniformity and colloidal stability of the synthesized sample.

3. Result and Discussion

3.1 Qualitative Phytochemical Screening:

The qualitative phytochemical screening of the aqueous leaf extract of *Alternanthera sessilis* revealed the presence of several bioactive secondary metabolites. Among the phytochemicals tested, flavonoids, terpenoids, anthraquinones, and glycosides were detected, whereas other tested metabolites were absent. These phytoconstituents are well known for their reducing, chelating, and stabilizing properties, which facilitate the green synthesis of metal nanoparticles.

Flavonoids and terpenoids play a significant role in reducing Zn^{2+} ions to ZnO nanoparticles and stabilizing the nanoparticle surface through their hydroxyl and carbonyl functional groups. Anthraquinones act as natural reducing agents and contribute to the formation of stable nanoparticles, while glycosides serve as capping agents, preventing particle aggregation and improving nanoparticle stability [18–20]. The presence of these phytochemicals confirms that the *A. sessilis* leaf extract provides the essential biomolecules required for the successful green synthesis of ZnO nanoparticles.

3.2. UV Visible Spectroscopy:

The optical properties of the biosynthesized ZnO nanoparticles were investigated using UV–Visible spectroscopy in the wavelength range of 200–800 nm. The UV–Vis absorption spectrum (Fig. 1) exhibited a strong absorption in the ultraviolet region, with maximum absorbance observed near 200–210 nm. The absorbance gradually decreased with increasing wavelength and remained nearly constant in the visible region (400–800 nm), indicating the high optical transparency of the synthesized ZnO nanoparticles. A broad absorption shoulder extending from approximately 250 to 320 nm was observed, which can be attributed to the intrinsic electronic transitions of ZnO and the influence of phytochemical molecules from the *Alternanthera sessilis* leaf extract adsorbed on the nanoparticle surface. The strong absorption in the ultraviolet region arises from the intrinsic electronic transition of ZnO, corresponding to the excitation of electrons from the valence band to the conduction band, which is a characteristic feature of wide band-gap semiconductor materials [21].

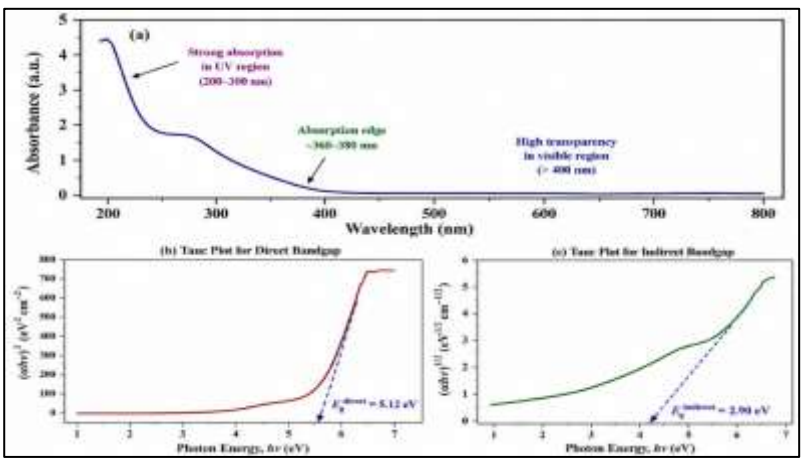

Figure 1: UV Vis spectroscopy analysis of ZnO NPs (a) UV-Vis absorbance spectrum (b) Direct Bandgap and (c) Indirect Bandgap.

3.3. Fourier transform infrared spectroscopy:

The FTIR spectrum of the synthesized sample was recorded in the range of 4000–400 cm^{-1} to identify the functional groups responsible for the reduction, stabilization and capping of the nanoparticles. The spectrum exhibited several characteristic absorption bands, indicating the presence of phytochemical constituents originating from the plant extract as well as the formation of the metal oxide nanoparticles (Fig 2). A broad absorption band observed in the 3200–3600 cm^{-1} region is attributed to the stretching vibration of hydroxyl (–OH) groups, which may arise from phenolic compounds, flavonoids and adsorbed water molecules. Weak bands around 2920–2850 cm^{-1} correspond to the asymmetric and symmetric stretching vibrations of aliphatic C–H groups, indicating the presence of organic molecules on the nanoparticle surface.

The absorption band near 1600–1650 cm^{-1} can be assigned to C=O stretching of amide groups or aromatic C=C vibrations, suggesting the involvement of proteins and polyphenolic compounds during nanoparticle synthesis. Peaks observed around 1380–1450 cm^{-1} are associated with C–N stretching and CH bending vibrations, while bands in the 1000–1200 cm^{-1} region correspond to C–O and C–O–C stretching vibrations of alcohols, ethers and polysaccharides. The most significant absorption band appearing in the low wavenumber region (approximately 400–600 cm^{-1}) is attributed to the Zn–O stretching vibration, confirming the successful formation of ZnO nanoparticles [22]. The presence of hydroxyl, carbonyl and other oxygen-containing functional groups indicates that biomolecules present in the *Alternanthera sessilis* leaf extract acted as reducing and stabilizing agents during the green synthesis process.

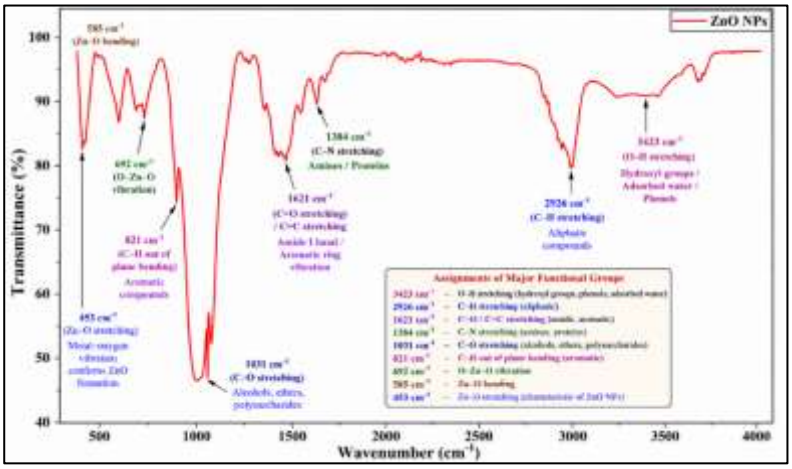

Figure 2: FTIR transmittance spectrum of ZnO NPs

3.4. X-ray diffractogram:

The XRD pattern of the green synthesized ZnO nanoparticles exhibited characteristic diffraction peaks at 2θ values of 31.7°, 34.4°, 36.2°, 47.5°, 56.6°, 62.9°, 66.4°, 67.9°, 72.4°, 76.9°, 81.1° and 89.4°**,** corresponding to the (100), (002), (101), (102), (110), (103), (200), (112), (201), (004), (202) and (104) crystal planes, respectively. These diffraction peaks are in good agreement with the standard hexagonal wurtzite ZnO phase (JCPDS Card No. 03-065-0523**)**, confirming the successful formation of crystalline ZnO nanoparticles. The absence of impurity peaks indicates the high phase purity of the synthesized ZnO nanoparticles. The average crystallite size was calculated using the Debye–Scherrer equation from the most intense (101) diffraction peak and was found to be 22.8 nm. The sharp diffraction peaks and small crystallite size demonstrate the high crystallinity of the biosynthesized ZnO nanoparticles, making them suitable for photocatalytic and biomedical applications [23].

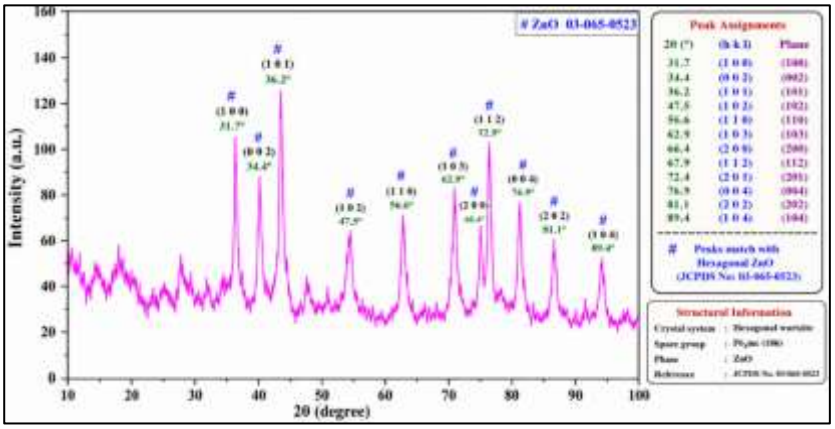

Figure 3: X-ray diffractogram of ZnO NPs

3.5. FESEM-EDAX analysis:

The surface morphology of the green synthesized ZnO nanoparticles was examined by FESEM, while the elemental composition was confirmed by EDAX analysis (Figure 4). The FESEM micrograph revealed that the ZnO

nanoparticles were predominantly spherical to quasi-spherical in shape with slight agglomeration. The observed agglomeration is attributed to the high surface energy of the nanoparticles and the interaction of phytochemicals from the *Alternanthera sessilis* leaf extract, which act as reducing and capping agents during synthesis. The nanoparticles were uniformly distributed with a rough surface morphology, indicating the successful formation of ZnO nanoparticles. The average particle size estimated from FESEM image analysis was approximately 23–35 nm. The EDAX spectrum confirmed the elemental composition of the synthesized nanoparticles. Strong characteristic peaks corresponding to Zn and O verified the successful formation of ZnO nanoparticles. In addition, weak signals of C, Cl, Na, Mg, Si, and Al were observed. The carbon peak originated from organic phytochemicals adsorbed on the nanoparticle surface, whereas the trace amounts of Cl, Na, Mg, Si and Al are attributed to plant-derived biomolecules, residual precursor salts, glassware or sample preparation [24]. The absence of impurity peaks from other metals indicates the high purity of the biosynthesized ZnO nanoparticles.

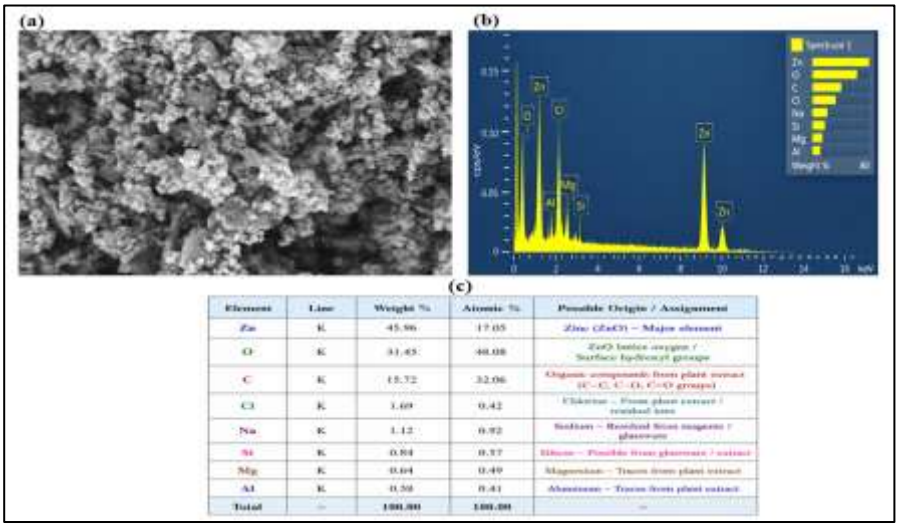

Figure 4: Morphology and Elemental distribution (a) FESEM micrograph (b) EDAX spectrum and (c) EDAX composition.

3.6. HRTEM analysis:

The morphology and microstructure of the biosynthesized ZnO nanoparticles were investigated by HRTEM (Fig. 5). The HRTEM images revealed that the nanoparticles were predominantly spherical to quasi-spherical in shape with slight agglomeration. The particle size distribution ranged from 3 to 35 nm, with an average particle size of 23–35 nm, which is in good agreement with the FESEM analysis. High-resolution images exhibited well-defined lattice fringes, confirming the crystalline nature of the synthesized ZnO nanoparticles. The measured interplanar spacings (d-spacing) of 0.281, 0.260 and 0.247 nm were assigned to the (100), (101) and (002) crystallographic planes, respectively, which are characteristic of the hexagonal wurtzite ZnO crystal structure and are in agreement with the XRD results (JCPDS No. 03-065-0523). The selected area electron diffraction (SAED) pattern displayed distinct concentric diffraction rings indexed to the (100), (002), (101), (102), (110) and (103) planes, confirming the polycrystalline nature of the ZnO nanoparticles. The FFT pattern further verified the crystallinity and lattice orientation of the nanoparticles [25,26].

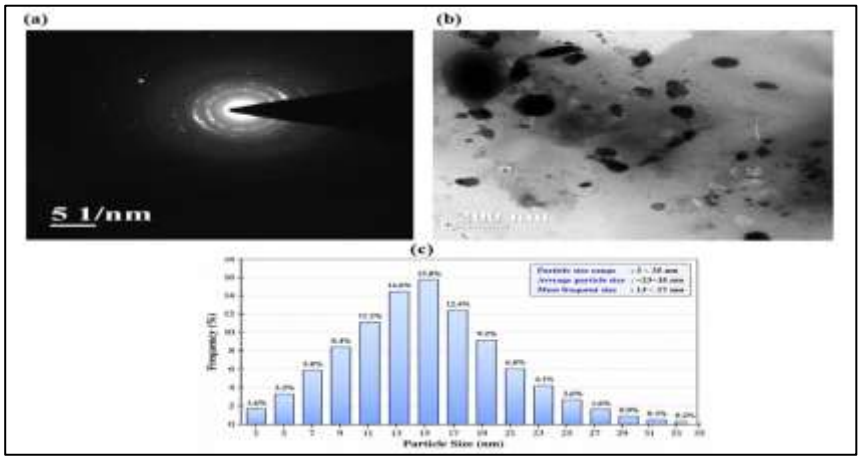

Figure 5: Morphology and Size Distribution (a) SAED pattern (b) HRTEM micrograph and (c) Particle size distribution histogram.

3.7. Dynamic Light Scattering (DLS) and Zeta Potential Analysis:

The DLS analysis (Fig. 6a) showed a multimodal particle size distribution, with the major hydrodynamic particle size centered around 900–1200 nm, indicating aggregation of ZnO nanoparticles in aqueous suspension. The larger size

obtained by DLS compared to FESEM and HRTEM is due to the measurement of the hydrodynamic diameter and particle agglomeration. The zeta potential analysis (Fig. 6b) exhibited a single peak at approximately −7.9 mV, indicating a moderately negative surface charge and moderate colloidal stability. The negative surface charge is attributed to the adsorption of phytochemicals from *Alternanthera sessilis*, which act as natural capping and stabilizing agents [27].

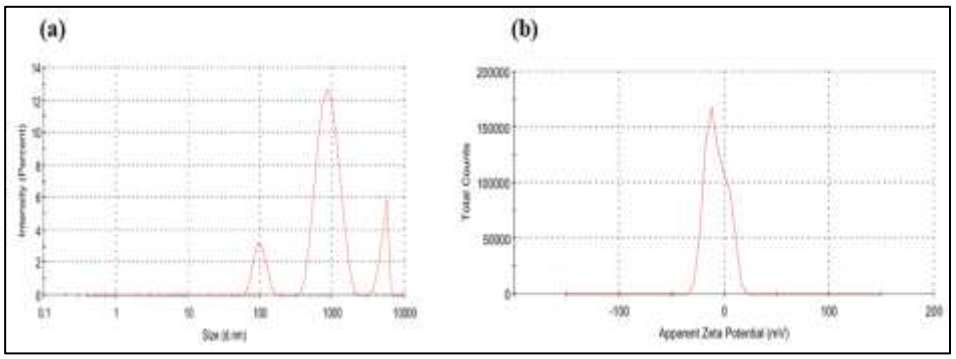

Figure 6: Dynamic Light Scattering (a) Zeta Size and (b) Zeta potential

Conclusion

In this study, ZnO nanoparticles were successfully synthesized through a simple and eco-friendly green synthesis approach using the aqueous leaf extract of *Alternanthera sessilis*. The presence of flavonoids, terpenoids, anthraquinones, and glycosides in the plant extract facilitated the reduction and stabilization of ZnO nanoparticles. UV–Visible and FTIR analyses confirmed the optical properties and the involvement of plant-derived functional groups during nanoparticle formation. XRD analysis demonstrated the formation of highly crystalline hexagonal wurtzite ZnO with an average crystallite size of 22.8 nm. FESEM and HRTEM analyses revealed spherical to quasi-spherical nanoparticles with sizes ranging from 3 to 35 nm, while EDAX confirmed the elemental purity of the synthesized material. DLS and zeta potential analyses indicated moderate colloidal stability in aqueous suspension. The results demonstrate that *A. sessilis* is a promising natural resource for the sustainable production of ZnO nanoparticles. The synthesized nanoparticles possess desirable structural, morphological, and optical properties, making them suitable for further investigation in photocatalytic, antimicrobial, antioxidant, and other biomedical applications.

References

1. S. Bayda, M. Adeel, T. Tuccinardi, M. Cordani, F. Rizzolio, The History of Nanoscience and Nanotechnology: From Chemical–Physical Applications to Nanomedicine, Molecules 25 (2019). https://doi.org/10.3390/molecules25010112.
2. N. Alsaiari, F. Alzahrani, A. Amari, H. Osman, H. Harharah, N. Elboughdiri, M. Tahoon, Plant and Microbial Approaches as Green Methods for the Synthesis of Nanomaterials: Synthesis, Applications, and Future Perspectives, Molecules 28 (2023). https://doi.org/10.3390/molecules28010463.
3. N.B. Singh, B. Kumar, U.L. Usman, M.A.B.H. Susan, Nano revolution: Exploring the frontiers of nanomaterials in science, technology, and society, Nano-Structures & Nano-Objects (2024). https://doi.org/10.1016/j.nanoso.2024.101299.
4. J. Jeevanandam, S.F. Kiew, S. Boakye-Ansah, S. Lau, A. Barhoum, M. Danquah, J. Rodrigues, Green approaches for the synthesis of metal and metal oxide nanoparticles using microbial and plant extracts., Nanoscale (2022). https://doi.org/10.1039/d1nr08144f.
5. G. Edo, A. Mafe, A. Ali, P. Akpoghelie, E. Yousif, E. Isoje, U. Igbuku, K. Zainulabdeen, J. Owheruo, A. Essaghah, H. Umar, D. Ahmed, A. Alamiery, Eco-friendly Nanoparticle Phytosynthesis via Plant Extracts: Mechanistic Insights, Recent Advances, and Multifaceted Uses, Nano TransMed (2025). https://doi.org/10.1016/j.ntm.2025.100080.
6. Z. Villagrán, L. Anaya-Esparza, C. Velázquez-Carriles, J. Silva-Jara, J. Ruvalcaba-Gómez, E. Aurora-Vigo, E. Rodríguez-Lafitte, N. Rodríguez-Barajas, I. Balderas-León, F. Martínez-Esquivias, Plant-Based Extracts as Reducing, Capping, and Stabilizing Agents for the Green Synthesis of Inorganic Nanoparticles, Resources (2024). https://doi.org/10.3390/resources13060070.
7. V. Soni, P. Raizada, P. Singh, H. Cuong, R. S., A. Saini, R. Saini, Q. Van Le, A. Nadda, T. Le, V. Nguyen, Sustainable and green trends in using plant extracts for the synthesis of biogenic metal nanoparticles toward environmental and pharmaceutical advances: A review., Environ. Res. (2021) 111622. https://doi.org/10.1016/j.envres.2021.111622.
8. H. Singh, M. Desimone, S. Pandya, S. Jasani, N. George, M. Adnan, A. Aldarhami, A. Bazaid, S. Alderhami, Revisiting the Green Synthesis of Nanoparticles: Uncovering Influences of Plant Extracts as Reducing Agents for Enhanced Synthesis Efficiency and Its Biomedical Applications, Int. J. Nanomedicine 18 (2023) 4727–4750. https://doi.org/10.2147/ijn.s419369.
9. M. El-Saadony, G. Fang, S.-M. Yan, S. Alkafaas, M. El Nasharty, S. Khedr, A.M. Hussien, S. Ghosh, M. Dladla, S. Elkafas, E. Ibrahim, H. Salem, W. Mosa, A. Ahmed, D. Mohammed, S. Korma, M. El-Tarabily, A. Saad, K. El-Tarabily, S. AbuQamar, Green Synthesis of Zinc Oxide Nanoparticles: Preparation, Characterization, and Biomedical Applications - A Review, Int. J. Nanomedicine 19 (2024) 12889–12937. https://doi.org/10.2147/ijn.s487188.
10. S. Alamdari, S. Ghamsari, C. Lee, W. Han, H. Park, M. Tafreshi, H. Afarideh, M. Ara, Preparation and Characterization of Zinc Oxide Nanoparticles Using Leaf Extract of Sambucus ebulus, Appl. Sci. (2020).

https://doi.org/10.3390/app10103620.
11. F. Rahman, M.A.M. Patwary, M.A.B. Siddique, M. Bashar, M.A. Haque, B. Akter, R. Rashid, M.A. Haque, A.R. Uddin, Green synthesis of zinc oxide nanoparticles using Cocos nucifera leaf extract: characterization, antimicrobial, antioxidant and photocatalytic activity, R. Soc. Open Sci. 9 (2022). https://doi.org/10.1098/rsos.220858.
12. M. Al-Darwesh, S. Ibrahim, M. Mohammed, A Review on Plant Extract Mediated Green Synthesis of Zinc oxide Nanoparticles and Their biomedical Applications, Results Chem. (2024). https://doi.org/10.1016/j.rechem.2024.101368.
13. A. Mandal, S. Katuwal, F. Tettey, A. Gupta, S. Bhattarai, S. Jaisi, D. Bhandari, A. Shah, N. Bhattarai, N. Parajuli, Current Research on Zinc Oxide Nanoparticles: Synthesis, Characterization, and Biomedical Applications, Nanomaterials 12 (2022). https://doi.org/10.3390/nano12173066.
14. R. Hamed, R. Obeid, R. Abu-Huwaij, Plant mediated-green synthesis of zinc oxide nanoparticles: An insight into biomedical applications, Nanotechnol. Rev. 12 (2023). https://doi.org/10.1515/ntrev-2023-0112.
15. J. Singh, T. Dutta, K. Kim, M. Rawat, P. Samddar, P. Kumar, 'Green' synthesis of metals and their oxide nanoparticles: applications for environmental remediation, J. Nanobiotechnology 16 (2018). https://doi.org/10.1186/s12951-018-0408-4.
16. S. Faisal, H. Jan, S. Shah, S. Shah, A. Khan, M.T. Akbar, M. Rizwan, F. Jan, Wajidullah, N. Akhtar, A. Khattak, S. Syed, Green Synthesis of Zinc Oxide (ZnO) Nanoparticles Using Aqueous Fruit Extracts of Myristica fragrans: Their Characterizations and Biological and Environmental Applications, ACS Omega 6 (2021) 9709–9722. https://doi.org/10.1021/acsomega.1c00310.
17. M. Naseer, U. Aslam, B. Khalid, B. Chen, Green route to synthesize Zinc Oxide Nanoparticles using leaf extracts of Cassia fistula and Melia azadarach and their antibacterial potential, Sci. Rep. 10 (2020). https://doi.org/10.1038/s41598-020-65949-3.
18. A. Marukurti, A.M. Reddy, S.R. Medapalli, P.B. Kasi, P.T. Rao, R. Anupoju, D. Ramachandran, B. Mallikarjuna, K. Sarojani, P.V. Nirmala, Evaluation of anti-vibriocidal, antioxidant properties and cytotoxicity of bio fabricated/green synthesized silver nanoparticles using Euphorbia hitra L. leaf extract, Next Mater. 7 (2025) 100355. https://doi.org/https://doi.org/10.1016/j.nxmate.2024.100355.
19. P.T. Rao, A. Marukurti, V.N. Pangi, B.D. Lakshmi, B. Mallikarjuna, K.S. Chandra, R.K. Ramachandra, Preparation and biophysical characterisation of Ag-Cu bimetallic nanoparticles, Discov. Appl. Sci. 7 (2025) 1246. https://doi.org/10.1007/s42452-025-07425-z.
20. A. Marukurti, A.M. Reddy, P.V. Nirmala, D. Kalyani, K. Ramaneswari, I.J.N. Padmavathi, L.P. Pemmaraju, G.S. Silvanus, B.S. Keerthana, S. Farhana, D. Ramachandran, B. Mallikarjuna, P.B. Kasi, In vitro biological activities of silver nanoparticles using methanolic leaf extract of Plumeria rubra, Sci. Rep. 15 (2025) 28303. https://doi.org/10.1038/s41598-025-14353-w.
21. E. Silva, V.M. Orozco-Carmona, A. Castro-Beltran, P.A. Luque, Structural and optical properties of semiconductor ZnO nanoparticles synthesized using Rubus glaucus extract for enhanced photocatalytic activity, Appl. Phys. A 130 (2024) 369. https://doi.org/10.1007/s00339-024-07519-2.
22. K.S.L. Krishna, B. Nageshwari, D. Kalyani, R. Merugu, Sustainable synthesis of ZnO/carbon dots nanocomposites and evaluation of antimicrobial, in vitro antioxidant and anti-inflammatory properties, Next Res. 2 (2025) 100791. https://doi.org/https://doi.org/10.1016/j.nexres.2025.100791.
23. L. Mechi, H. Chemingui, J. Chékir, A.K.D. Alsukaibi, H. Azaza, M. Mhiri, Plant mediated green synthesis of zinc oxide nanoparticles for photocatalytic degradation of trypan blue: Optimisation via box-Behnken design, Results Chem. 18 (2025) 102822. https://doi.org/https://doi.org/10.1016/j.rechem.2025.102822.
24. V.N. Pangi, A. Marukurti, A.M. Reddy, S.R. Medapalli, Synthesis of Biogenic Silver Nanoparticles (bAgNPs) Using Leaf Extract of Mirabilis jalapa and Evaluation of Anti-vibriocidal, Anti-oxidant properties and Cytotoxicity, Bionanoscience (2023). https://doi.org/10.1007/s12668-023-01060-x.
25. R. Maind, S. Halder, A.R. Bhat, D. Bhattacharya, M.H. Mujahid, A. Abu-Rayyan, M. Iqbal, V.J. Upadhye, S. Ahmed, M. Alam, G. Tataringa, Biomimetic green synthesis of ZnO nanoparticles using Cheilocostus speciosus and Gardenia gummifera with comprehensive characterization and bioactivity assessment, Sci. Rep. 15 (2025) 44323. https://doi.org/10.1038/s41598-025-30720-z.
26. G. Singh, V. Kumar, J. Gaur, S. Kumar, Sustainable Hydrothermal Route for ZnO Nanoparticles using Berseem extract: A Structure–Property Correlation Study, ICCK Trans. Adv. Funct. Mater. Process. 1 (2025) 68–77. https://doi.org/10.62762/TAFMP.2025.399354.
27. S. Bhattacharjee, DLS and zeta potential - What they are and what they are not?, J. Control. Release Off. J. Control. Release Soc. 235 (2016) 337–351. https://doi.org/10.1016/j.jconrel.2016.06.017.